EUROPHYSICS LETTERS 1 December 2000

Europhys. Lett., **52** (5), pp. 532–538 (2000)

Folding of viscous sheets and filaments

M. Skorobogatiy[1] and L. Mahadevan[2](*)

[1] *Departments of Physics, Massachusetts Institute of Technology*
77 Mass. Ave., Cambridge, MA 02139, USA
[2] *Department of Mechanical Engineering, Massachusetts Institute of Technology*
77 Mass. Ave., Cambridge, MA 02139, USA

(received 26 June 2000; accepted in final form 4 October 2000)

PACS. 47.20.Gv – Viscous instability.
PACS. 91.45.Ty – Folds and Folding.
PACS. 47.50.+d – Non-Newtonian fluid flows.

Abstract. – We consider the nonlinear folding behavior of a viscous filament or a sheet under the influence of an external force such as gravity. Everyday examples of this phenomenon are provided by the periodic folding of a sheet of honey as it impinges on toast, or the folding of a stream of shampoo as it falls on one's hand. To understand the evolution of a fold, we formulate and solve a free-boundary problem for the phenomenon, give scaling laws for the size of the folds and the frequency with which they are laid out, and verify these experimentally.

The buckling of solids is a well-established subject whose origins date back to the work of Euler and Bernoulli. This instability, which arises as a result of the competition between axial compression and bending in slender objects, is not restricted to solids; it can also occur in creeping flows of fluids in slender geometries. As in the case of solids, the buckling, folding, and coiling of thin sheets and filaments of fluids occurs on length scales spanning several orders of magnitude, including phenomena from geophysics [1] to materials processing [2], see fig. 1. Everyday examples of this phenomenon abound. In the kitchen, a sheet of honey, maple syrup or cake batter poured onto a surface from a sufficient height is laid out in a series of folds, while in the bathroom analogous phenomena can be observed with shampoo. A related phenomenon occurs when a falling filament coils steadily on impact, and has been recently analyzed in [3]. However, unlike the coiling, folding is inherently unsteady, involves a somewhat subtle moving contact line problem, and is the consequence of the competition between viscous and gravitational forces.

In this letter, we consider the folding of a filament confined to lie in a vertical plane, fig. 1c, and later show how the results can be transposed to the problem of the folding of a viscous sheet. Observations show that when a thin viscous soap film is stretched in a vertical frame, a drop of soap falling through it is pulled out into a filament that forms a series of periodic folds at the bottom of the frame. The physical parameters governing the phenomena include the density ρ and viscosity μ of the fluid (kinematic viscosity $\nu = \mu/\rho$), the flow rate Q, gravity

(*) E-mail: l_m@mit.edu

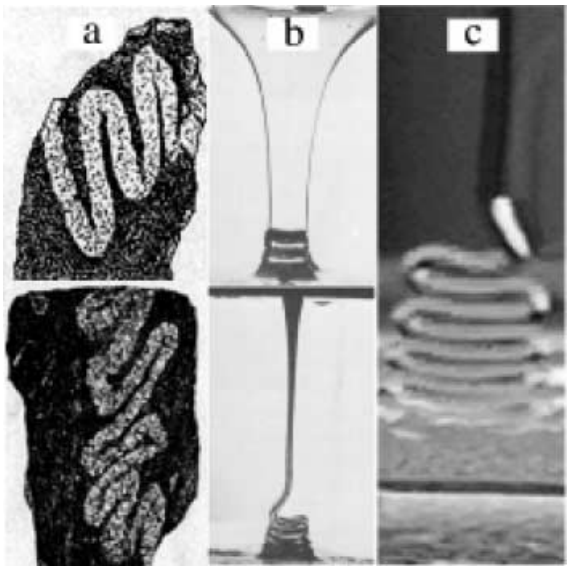

Fig. 1

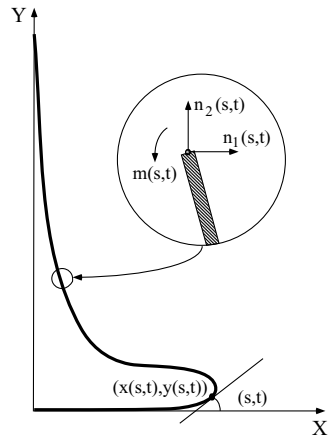

Fig. 2

Fig. 1 – Some instances of viscous folding. (a) Folds in rock formations have typical wavelengths of the order of 20 cm (from [4]). (b) Two views of the folding of a sheet of silicone oil of viscosity 1 Pa s. (c) A viscous soap filament falling vertically in a thin soap film folds periodically. In the last two examples, the typical fold length is of the order of a few mm.

Fig. 2 – A schematic of a viscous filament of constant diameter folding and flowing under the influence of gravity. At time t, the filament is described by its center line $x(s,t), y(s,t)$, and the orientation of its cross-section $\phi(s,t)$, the angle between the tangent to the center line and the horizontal, s being the arc length. $n_1(s,t)$, $n_2(s,t)$ and $m(s,t)$ are the depth-integrated stress and moment resultants described in the text.

g, a characteristic filament radius r and the height h from which the filament falls. As h is gradually increased, the axial stagnation flow becomes unstable to bending disturbances and the filament is laid out in a series of periodic folds of length L at a frequency Ω. The onset of the instability is determined by the relative magnitude of a gravitational time scale $(h/g)^{1/2}$ and a viscous time scale $r^2\rho/\mu$ characterized by a Reynolds number $Re = gr^3/\nu^2$. A similar parameter $\rho g h^3/B$, where B is the bending stiffness, occurs in the elastic analogue [5]. Only below a critical value of the aspect ratio of the filament r/h or Re [6] is the axisymmetric stagnation flow unstable. Far from onset, when r/h becomes sufficiently small, the flow is still mainly an axial stretching flow corresponding to the "outer" region [7]. However, in a small neighbourhood of the bottom frame there is a "bending boundary layer", where the filament diameter is constant, although its center line is highly curved, as seen in fig. 1b and c. For the low folding frequencies that are typically observed, filament inertia is unimportant since $\Omega \ll (\frac{g}{L})^{1/2}$ [8]; then the dynamics of folding are determined by the balance between the forces due to gravity and viscosity.

Folding occurs in various stages and is reminiscent of an analogous phenomenon that occurs when an elastic sheet is fed towards a surface [5]. The filament buckles on contact with the bottom frame (horizontal surface); further flow causes the filament to form a contact point where it is tangential to the horizontal surface. As an incipient fold is laid out, this contact

point moves away from the vertical line of feeding. Under the influence of gravity, the filament eventually folds back on itself forming a second contact point. The filament may then roll briefly about this new contact point until the curvature at this contact point vanishes; what is more common is that it simply sinters with the previous fold. In either case, a third contact point begins to move from this location towards the vertical feeding line until it is directly below the feeding point, leading to the formation of a half-fold. An identical scenario on the opposite side leads to the formation of the second half of the periodic fold. The next fold is laid out on the previous one; if the height from which the filament is fed is large compared to the height of the fold, we only need to consider the formation of a single fold.

In the folding regime, the filament is assumed to have a circular cross-section of constant diameter [9] with its center line confined to two dimensions allowing us to characterize the filament center line at time t in terms of its arc-length s and the angle $\phi(s,t)$ between the tangent to the center line and the x-axis. Letting $n_1(s,t)$ and $n_2(s,t)$ be the integrated stress resultants in the x and y directions and $m(s,t)$ be the bending moment in the z-direction (fig. 2), the balance of horizontal and vertical forces, and moments leads to

$$\begin{aligned} n_{1s} &= 0, \qquad n_{2s} = \pi r^2 \rho g, \\ m_s &= n_1 \sin\phi - n_2 \cos\phi \end{aligned} \tag{1}$$

where $(\cdots)_s = \partial(\cdots)/\partial s$. Here we have neglected the inertia of the filament which is being fed at velocity v. The total length of the filament under consideration is vt, so that $0 \le s \le vt$.

These equations are 1-dimensional approximations to the 3-dimensional equations of equilibrium and are valid for a slender filament in the long-wavelength limit. For completeness, they must be supplemented by a fourth equation relating the variables n_1, n_2, m, ϕ. Since the dominant mode of deformation of the filament during folding is due to bending, a natural candidate is a relation between the curvature $\phi_s(s,t)$ and the torque. For a slender elastic filament, the axial strain ϵ due to bending varies linearly with the transverse dimension y measured from its central (neutral) surface, and inversely with the radius of curvature [10], so that the stress $\sigma \sim E y \phi_s$. Integrating the stress through the cross-section leads to a vanishing resultant; however the moment $m \sim \int \sigma y \mathrm{d}A$ does not vanish, and yields $m \sim E r^4 \phi_s$. For a constant-diameter viscous filament flowing around a bend (see fig. 1c), the axial stress which is proportional to the strain rate is given by $\sigma \sim \mu (y\phi_s)_t \sim \mu y \phi_{st}$. Therefore, for a viscous filament, $m \sim \mu r^4 \phi_{st}$. This heuristic argument can be formalized as a leading-order asymptotic theory for the creeping flow of a slender filament of small aspect ratio following [11], and leads to

$$m = \frac{3}{4} \pi \mu r^4 \phi_{st} \,. \tag{2}$$

Equations (1), (2) are sufficient to determine ϕ, n_1, n_2; we note that the stress resultants n_1, n_2 are determined by the boundary conditions and in fact are Lagrange multipliers that enforce the constraints of inextensibility and vanishing transverse velocity gradients. Upon defining the dimensionless variables $\bar{s} = \frac{s}{h}, \bar{t} = \frac{tv}{h}, \bar{n}_{1,2} = \frac{n_{1,2}}{\pi r^2 \rho g h}$, with h being the height from which the filament is being "fed" by the axial flow, eqs. (1), (2) can be rewritten, on dropping the bars, as

$$\begin{aligned} n_{1s} &= 0, \qquad n_{2s} = 1 \,, \\ \eta \phi_{sst}(s,t) &= n_1 \sin\phi - n_2 \cos\phi \,, \end{aligned} \tag{3}$$

where $\eta = 3\mu r^2 v / 4\rho g h^4$ is a scaled viscous bending resistance, and we start the clock when the filament first touches the bottom plate so that $0 \le s \le 1 + t$. The shape of the filament at any instant is determined by integrating the two kinematic relations $x_s = \cos\phi, y_s = \sin\phi$.

In a typical experiment, $\mu \sim 10\,\mathrm{Pa\,s}$, $r = 10^{-3}\,\mathrm{m}$, $v = 0.1\,\mathrm{m/s}$, $\rho = 10^3\,\mathrm{kg/m^3}$, $h = 0.1\,\mathrm{m}$, so that $\eta \sim 10^{-6}$. This singularly perturbed PDE has two bending boundary layers confined to the feeding point and a small neighborhood of the horizontal surface, where the fold is laid out. During the evolution of a fold, the boundary conditions must be specified at the unknown contact points, and change at certain critical times as new contact lines are born. To facilitate the numerical solution of this problem, we follow [5] and keep the domain of the problem fixed to $s \in [0,1]$, rescaling all lengths by defining $\xi = \frac{s}{l_i+(t-t_i)+(s_i(t_i)-s_i(t))}$, where $s_i(t)$ is the location of the i-th contact point, l_i is the length of the filament between the latest contact point and the feeding point, and t_i denotes the time of birth of the i-th contact point [12]. Then the boundary conditions at the feeding point are

$$\begin{aligned} \phi(1,t) &= \frac{\pi}{2}\,, \\ x(1,t) = \int_0^1 \cos\phi(\xi,t)\mathrm{d}\xi &= -\frac{s_i(t)}{l_i+(t-t_i)+(s_i(t_i)-s_i(t))}\,, \\ y(1,t) = \int_0^1 \sin\phi(\xi,t)\mathrm{d}\xi &= \frac{1}{l_i+(t-t_i)+(s_i(t_i)-s_i(t))}\,. \end{aligned} \tag{4}$$

The first condition is due to the vertical feeding of the filament, while the second and third characterize the location of the feeding point as measured from the latest contact point $s_i(t)$. The boundary conditions at the contact point, which always lies on the same horizontal plane, vary with time. Once the filament has contacted the horizontal surface ($t = 0$), the filament buckles, and pivots about the point of contact $(0,0)$

$$\phi_\xi(0,t) = 0\,, \qquad x(0,t) = s_i(t)\,, \qquad y(0,t) = 0\,. \tag{5}$$

Here $s_0(t) = 0$ is the location of the contact point initially. We consider the formation of a fold as composed of two parts:

I) The filament becomes tangential to the surface at time $t = t_1$ and location $x = y = 0$. Further feeding causes the filament to be laid out as the contact point moves to $s = s_1(t)$. The location of the contact point $x(0,t) = s_1(t)$ is then determined by the condition of tangency

$$\phi(s_1(t),t) = 0, \phi_\xi(s_1(t),t) = 0\,. \tag{6}$$

II) As the feeding continues past $t = t_1$, the filament begins to dip downwards under its own weight until it touches itself on the horizontal frame for the first time at $t = t_2$, when a second contact point $s_2(t)$ is born. The filament can then roll about this contact point [5]. However, if the period of folding $1/\Omega$ is large compared to the time $\mu r/\sigma$ for surface tension to sinter the filament with the rest of the liquid at this location, this motion can be neglected. Then the part of the fold between $s_2(t)$ and $s_1(t)$ will not move at all and a new contact point moves away from $x = s_2(t)$, with the condition of tangency (6) replaced by

$$\phi(s_2(t),t) = \pi, \phi_\xi(s_2(t),t) = 0. \tag{7}$$

At time $t = t_3$ the contact line lies directly below the feeding point, thus completing the laying-out of half a period of the fold.

The nonlinear free-boundary problem (3)-(7) is solved using a finite-difference method which exhibits $O(\mathrm{d}t^2)$ accuracy in time and $O(\mathrm{d}\xi^4)$ in space. The integral boundary conditions (4) are implemented via a relaxation step using a damped Newton method; given a solution

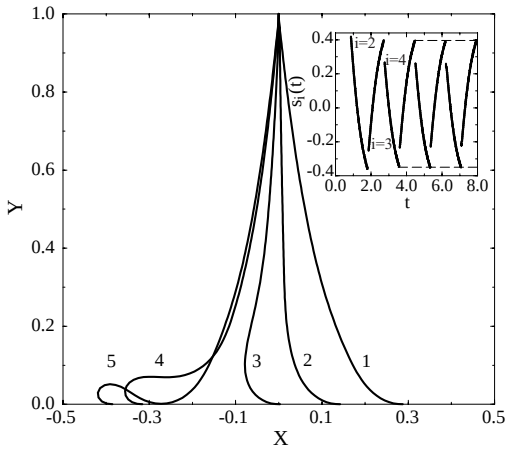

Fig. 3

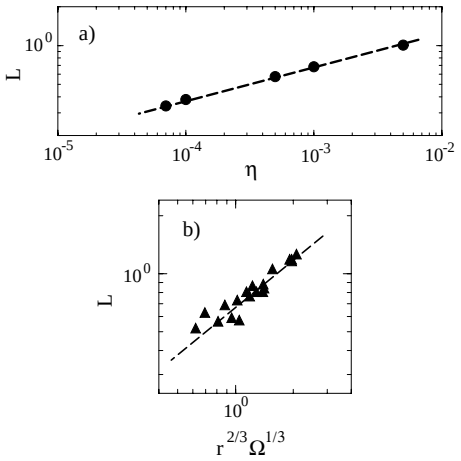

Fig. 4

Fig. 3 – The evolution of a half-period of a fold of a viscous filament constrained to move in a plane. Here $\eta = 10^{-4}$. The numbers denote the time sequence (in dimensionless units) $t_1 = 0.0$, $t_2 = 0.11$, $t_3 = 0.24$, $t_4 = 0.69$, $t_5 = 0.87$. Inset: The formation and evolution of the contact points during the folding of the filament. Here, we have neglected the piling-up of consecutive folds since their height is much smaller than the total height of fall of the filament. $s_i(t)$ denotes the location of the i-th contact line; periodicity is achieved after an initial transient of 2 folds. The apparent discontinuities in the contact line location simply denote the birth of new contact lines.

Fig. 4 – (a) The relation between the fold length L and η is fit well by the predicted power law $L \simeq \eta^{-0.24\pm0.04}$ for $\eta \ll 1$. (b) Experimental results corresponding to the folding of a soap filament, as shown in fig. 1c, reflecting fold lengths which vary from 0.52 to 1.3 cm, frequencies which vary from 1.5 to 11 Hz and filament diameters which vary from 0.021 to 0.085 cm. The data collapse is consistent with the theory which predicts $L_f \sim \Omega^{1/3} r^{2/3}$.

at time t, a new solution at time $t + \mathrm{d}t$ is calculated by using a relaxation step subject to the constraints (4). In following this evolution numerically, we start with an approximately straight filament as the initial condition and wait for several (3-5) periods until the influence of the initial conditions disappears and a periodic state is established. In fig. 3, we show the evolution of a half-period of the fold, for $\eta = 10^{-4}$. In fig. 3b we show the evolution of the contact lines that are formed during each period of the fold for the same value of η (10^{-4}) and see that the folding is indeed periodic after a short initial transient.

As η is decreased, the fold length also decreases, but rather slowly. For $\eta \ll 1$, a simple argument that balances viscous and gravitational forces reveals the nature of this dependence. In the neighborhood of a fold of length L, the filament turns around a bend of radius L at velocity v without a change in its diameter. This leads to an axial stretching stress that vanishes along the center surface of the filament and is linear in the depth, with a maximum that scales as $\mu r v/L^2$ so that the depth-integrated stress resultant vanishes. However the depth-integrated torque remains nonzero and scales as $\mu r^4 v/L^2$, being balanced by a gravitational torque of magnitude $\rho g r^2 L^2$. This leads to the following scaling laws for the fold length L and the folding frequency $\Omega \sim v/L$:

$$L \sim (\nu v r^2/g)^{1/4} \sim \eta^{1/4} h\,, \tag{8}$$

$$\Omega \sim (\nu r^2/g v^3)^{-1/4} \sim \eta^{-1/4} v/h\,. \tag{9}$$

To verify the scaling laws, we numerically evaluated the horizontal extent of the fold for various values of η. In fig. 4a, we show a plot of L *vs.* η, and see that $L \sim \eta^{0.24\pm0.04}$, which compares very well with the scaling law (8).

In a preliminary experimental venture to verify our theory, we have quantified the folding of soap filaments falling within a vertical soap film of thickness 0.1 mm stretched out in a frame of size 5 cm × 5 cm. The thin soap film drains very slowly compared to the rate at which a thick filament falls through it, eventually folding at the bottom (fig. 1c). By varying the flow rate, we were able to change the velocity and the thickness of the filament, and measure the frequency and length of the folds for a variety of filament diameters. In fig. 4b, we plot the dependence of the fold length L *vs.* $r^{2/3}\Omega^{1/3}$ for a range of folding frequencies and filament radii and see that the data collapses onto the power law $L \sim r^{2/3}\Omega^{1/3}$ that follows from (8), (9). Although even the crudest measurements are consistent with our simple theory, much remains to be done yet on the experimental front.

The folding of a sheet of constant width and thickness r can be similarly treated by replacing the viscous bending rigidity of the filament $3\pi\mu r^4/4$ in (2) by $\mu r^3/3$, the viscous bending rigidity of a sheet per unit width. However, in such cases (fig. 1b), surface tension causes the lateral edges to come together. For very viscous slow moving sheets, when $\mu v/\sigma \gg 1$, such as in some materials processing flows, our theory provides a very good starting point. We have also neglected the effect of the external fluid; our preliminary experiments show that this is a reasonable approximation. More generally, just as lubrication-type theories in hydrodynamics consider the varicose modes of the free surface, bending theories like the one here consider sinuous modes of the free surface. They correspond to the short-time pseudo-elastic behavior of a Newtonian fluid in slender geometries, and raise the question of other problems in the hydrodynamics of thin films that can be addressed using these ideas.

As an example, we consider the implications of our study on the folding of rocks and plates in geology [1, 13]. When a single layer of a highly viscous fluid is embedded in a less viscous environment that is subject to bulk shortening [14], a simple modification of the present theory suffices. This is easily done by including tangential and normal drag forces that are proportional to the velocity of the filament in the two directions in (1), while noting the anisotropy of the drag coefficients for the transverse and axial motion of slender bodies in a fluid. Nonlinear rheological properties may also be easily accounted for by changing the single constitutive equation (2). However, we leave these aspects for future examination.

* * *

We thank A. Tripathi and the McKinley Lab for help with some of the preliminary experiments on the folding of viscous sheets. LM thanks R. Fletcher for his detailed comments on the possible implications of these studies in geophysical problems and pointing out a number of relevant references including the works of Sederholm and Chapple. The Office of Naval Research supported this work through an NYI award to LM.

REFERENCES

[1] Johnson A. M. and Fletcher R. C., *Folding of Viscous Layers* (Columbia, New York) 1994.
[2] Yarin A. L., *Free Liquid Jets and Films: Hydrodynamics and Rheology* (Wiley) 1991.
[3] Mahadevan L., Ryu W. and Samuel A., *Nature*, **392** (1998) 140; **403** (2000) 502.
[4] Sederholm J. J., *Selected Works-Granites and Migmatites* (John Wiley and Sons, New York) 1967.

[5] Mahadevan L. and Keller J. B., *SIAM J. App. Math.*, **55** (1995) 1609; reprinted in *SIAM Rev.*, **41** (1999) 113.

[6] The nominal Reynolds number vr/ν must be scaled by $(h/r)^2$ to account for the different time scales for transverse (bending) and axial motions, and can in principle be large. However, in all the cases of interest here, the modified Reynolds number $vh^2/r\nu \ll 1$.

[7] For steady axial stretching flow of a filament in the absence of inertia and surface tension, integrating the Stokes' equations yields $3\mu(r^2u_z)_z = \rho g r^2$, where $r = r(z,t)$ is the radius of the filament at a vertical location z below the feeding point, and $u(z,t)$ is the axial velocity. When solved along with the continuity equation $Q = r^2u$, we get the outer solution for the flow velocity v and the filament diameter $2r$. Since the height of the folds is small compared to the total fall height, we can neglect it to a first approximation and solve the outer problem over the entire height of fall h. This solution provides the matching conditions to the inner problem of bending, which we focus on here.

[8] We refer here to filament inertia associated with the motion of the center line of the filament, which is not to be confused by the effects of fluid inertia that can enter due to motion with respect to the center line (which is small anyway).

[9] That the diameter is constant is a consequence of the large difference in time scales for transverse (bending) motions which occur on a time scale $(r/h)^2$ smaller than that for axial (stretching) motions, so that to leading order the filament bends without stretching or changing its diameter.

[10] Love A. E. H., *A Treatise on the Mathematical Theory of Elasticity*, 2nd edition (Dover) 1944.

[11] Buckmaster J., *J. Fluid Mech.*, **61** (1973) 449.

[12] Then eqs. (3) transform into $n_{1\xi} = 0, n_{2\xi} = (l_i + (t - t_i) + (s_i(t_i) - s_i(t))), \eta\phi_{\xi\xi t}(\xi,t) = \frac{2\eta(1-s_{it}(t))}{l_i+(t-t_i)+(s_i(t_i)-s_i(t))}\phi(\xi,t)_{\xi\xi} + (n_1\sin\phi(\xi,t) - n_2\cos\phi(\xi,t))(l_i + (t-t_i) + (s_i(t_i) - s_i(t)))^2$.

[13] Ramsay J. G., *Folding and Fracturing of Rocks* (McGraw-Hill) 1967.

[14] Chapple W. M., *Geol. Soc. Amer. Bull.*, **79** (1968) 47.